AIAA JOURNAL
Vol. 35, No. 8, August 1997

Finite Element Modeling of Open-Section Composite Beams with Warping Restraint Effects

Matthew W. Floros* and Edward C. Smith†
Pennsylvania State University, University Park, Pennsylvania 16802

A new finite element model is developed to capture spanwise torsion-related warping restraint effects in open-section composite beams. The new model features both twist and twist rate degrees of freedom, allowing for direct implementation of the kinematic boundary conditions associated with torsion-related warping restraints. A Vlasov cross-sectional model is used to determine the beam stiffness coefficients. The new model is validated against closed-form solutions for uniform composite I beams and detailed shell element solutions for more general spanwise geometries and loading conditions. A previous method of modeling spanwise torsion-related warping effects is reviewed and compared to the current model. Beams with spanwise taper, elastic couplings, and arbitrary warping boundary conditions are analyzed. Bending loads and distributed torsional loads are also investigated. Excellent correlation is observed between the current model, closed-form solutions, and finite element solutions. For beams with uniform cross-sectional and warping restraints at both ends, the global increase in torsional stiffness due to torsion-related warping effects is independent of distributed loadings. The stiffness increase was found to depend on the cross-sectional geometry in the vicinity of the restraint. For extremely slender beams, the new torsion model yields the classic St. Venant torsion solution.

Nomenclature

A, B, C	= arbitrary constants for mixed torsion differential equation
$\{D\}$	= element displacement vector
E_L, E_T	= Young's modulus in longitudinal and transverse directions
$EI_{\omega\omega}$	= beam warping stiffness
G_{LT}	= shear modulus of plies in principal direction
GJ	= beam torsion stiffness
$\{H\}$	= Hermitian shape function polynomial
$[K]$	= beam stiffness matrix
L	= beam length
$\{L\}$	= Lagrange shape function polynomial
M_x, M_y	= beam bending moments about x and y axes
M_ω	= bimoment applied to beam
m_ω	= applied external bimoment on beam
N	= axial force applied to beam
n	= applied external axial load to beam
$\{R\}$	= element load vector
T	= total torque applied to beam about z axis
T_s	= St. Venant torque applied to beam
t_s	= applied external St. Venant torsion load on beam
T_ω	= Vlasov torque applied to beam
(U, V, W)	= beam displacement coordinates in x, y, z
v_x, v_y	= applied external transverse loads on beam
(x, y, z)	= I-beam coordinate system
θ	= angle between s and x axes
λ	= warping stiffness parameter
ν_{LT}	= Poisson's ratio in principal plane
Π_p	= total element potential energy
Π_s	= strain energy for finite element
Π_s^*	= strain energy density for finite element
φ	= warping function
ϕ_y, ϕ_x, ϕ_z	= beam rotations about x, y, z axes
Ω	= potential of external loads
$(\ )'$	= differentiation with respect to z

Received Aug. 8, 1996; revision received Feb. 12, 1997; accepted for publication April 21, 1997.

*Graduate Assistant, Department of Aerospace Engineering, 233 Hammond Building. Member AIAA.
†Assistant Professor, Department of Aerospace Engineering. Member AIAA.

Introduction

OPEN-SECTION composite beams are used in a wide variety of aerospace applications. These structures exhibit high bending and axial stiffness with light weight and relatively low torsional stiffness. Analysis methods for bending and shear deformations of these sections are well documented. Long beams can be accurately modeled as Bernoulli–Euler beams, but for shorter beams and beams with bending-shear or extension-shear parasitic couplings, transverse shear deformations must be included in the analysis.

Similarly, the torsional behavior of long, slender beams can be accurately described with St. Venant torsion theory. For lower aspect ratio beams, torsion-related warping effects become significant, and both St. Venant and Vlasov torsion must be used. Recently, it has been shown that warping restraint effects can be significant in moderate or even large aspect ratio composite beams.[1] Significant errors in torsional response can result if warping effects are ignored.

A common application of open-section composite beams is the bearingless rotor flexbeam in advanced helicopter rotor systems. Several major helicopter manufacturers (Bell, Boeing, McDonnell–Douglas, Sikorsky, and MBB—Deutsche Aerospace) have been producing a number of bearingless main rotor and tail rotor designs utilizing open-section, moderate aspect ratio composite beams.[2–6] Newer designs may feature elastically tailored laminates, coupling complex bending and twisting motions together for improved damping, reduced vibration, enhanced performance, and higher stability margins. I beams are well suited for elastic tailoring applications because angle plies in the separated flanges allow for larger extension–twist or bending–twist couplings.

Elastic couplings can make analysis of both the fixed- and rotary-wing aircraft structures more complex. Effects such as torsion-related warping can play an important role in beam response and must be addressed both in the cross-sectional analysis and the spanwise discretization. Progress on cross-sectional modeling of beams with elastic couplings has been ongoing for many years, but studies have not focused on spanwise discretization in the past. An extremely accurate cross-sectional model is not very useful unless it can be extended into the spanwise dimension. This work focuses on developing a new spanwise discretization model that is capable of accurately representing warping restraint effects in composite beams.

The first work with the contour-based cross-sectional analysis methods used in this study was conducted by Vlasov.[7] A textbook including warping of thin-walled structures was written more recently by Gjelsvik.[8] The Vlasov theory in these books could model thin-walled beams by translating the two-dimensional

plate stress resultants and displacements to one-dimensional beam forces, moments, and displacements. In this way, loads and displacements are only a function of the spanwise coordinate. The theory was useful for modeling generally shaped thin-walled isotropic sections. Examples of both open and closed sections were included.

Vlasov theory was initially extended to composites by Bauld and Tzeng.[9] Only symmetric laminates were considered, and transverse shear was not taken into account. Chandra and Chopra[1] included transverse shear effects of the beam, although transverse shear of the individual laminates in the cross section was not considered. Bending–torsion coupled beams were considered. Closed-form solutions for uniform I beams under tip bending and torsional loadings were developed and tested against experimentally determined results. The study showed that unlike isotropic beams, composite beams with large aspect ratios (on the order of 60) were strongly affected by warping restraints. The theory was later extended to include closed sections.[10,11]

Bauchau and Chiang[12] utilized a nonlinear shell element model including warping effects in an analysis of tail rotor blades. The effects of warping on rotating natural frequencies were considered. Another beam theory was proposed, which expanded the warping terms in a series of eigenwarpings, assuming that the beam cross section is infinitely rigid in its own plane. Thin-walled box beam sections were analyzed and compared to classical results.[13]

Kosmatka[14] formulated a nonlinear theory for spinning anisotropic beams including warping effects. Cylindrical cases were examined with varying ply orientations and slenderness ratios. Results showed that for the cases examined, warping effects influenced the torsion natural frequencies, but not bending.[14] Another study was conducted to determine the behavior of antisymmetric beams with initial twist. Rectangular cross sections were examined.[15]

Crawley and Dugundji[16] and Jensen et al.[17] conducted studies on in-plane warping of isotropic[16] and bending–torsion coupled[17] composite plates. A partial Ritz method was used assuming a chordwise deflection shape. For bending–torsion coupled cases, natural frequencies were significantly affected by excluding the chordwise deflection.

Two-dimensional methods have also been developed to describe torsion-related warping. Lee and Kim[18] and Stemple and Lee[19] used a warping nodes method, where the cross section is descretized and the out-of-plane deformation at each point is calculated. These methods yield accurate results but require too many degrees of freedom to be practical for aeroelastic analysis.

Yuan et al.[20] formulated a beam finite element approach where the warping magnitude was considered as an independent degree of freedom. The principal focus of this study was aeroelastic stability, and no efforts were reported to evaluate the warping model.

Another modeling approach is to artificially modify the torsional stiffness of the beam near a warping restraint to capture the boundary-layer effect (modified-GJ method). Nixon[21] used this method for an analysis of extension–torsion coupled rotor blades. The stiffness modification is based on closed-form solutions developed in Ref. 8.

Tracy and Chopra[22,23] derived two different torsion stiffness modifications to capture warping effects as part of a study on aeroelastic stability of bearingless composite rotor systems. These modifications were based on the closed-form solutions for uniform beams developed in Ref. 1. Stiffness modifications are dependent on loadings and boundary conditions. Results for tip-loaded beams with uniform cross sections were presented.

The objective of this research is to develop a new method of incorporating restrained warping effects into beam finite elements. The formulation is intended to be used for applications such as aeroelastic response and stability calculations, where linear beam finite elements with distinct bending, torsion, and extension degrees of freedom are typically used. In such calculations, closed-form results lack the capability of modeling real structures and loading conditions. Shell element results, though accurate, require computation times on the order of minutes rather than seconds for a beam model. The current work proposes a model that is both computationally simple and accurate for structures with complex loadings, spanwise taper, and elastic couplings.

Analytical Formulation

This section briefly describes torsion-related warping, the Vlasov cross section model, and the formulation of the mixed torsion element. The element is compared to a previous approach for modeling torsion-related warping in beam elements that has been implemented in past aeroelastic analyses. The improvements over the previous approach are noted.

Torsion-related warping is a deformation in which the cross section deforms locally out-of-plane, but does not produce a net axial deformation (see Fig. 1). The axial deflection w due to warping is proportional to a warping function and the spanwise rate of twist in the beam,

$$w(z, s) = \varphi(s)\phi_z'(z) \tag{1}$$

For an isotropic beam, the governing differential equation for a beam with mixed torsion is

$$EI_{\omega\omega}\phi_z''' - GJ\phi_z' = -(T_s + T_\omega) \tag{2}$$

where $EI_{\omega\omega}$ is the warping stiffness, GJ is the torsion stiffness, and $(T_s + T_\omega)$ is the applied torque. The applied torque is the sum of St. Venant torque T_s and Vlasov torque T_ω. The Vlasov torque is a consequence of the so-called warping moment or bimoment M_ω. The bimoment has units of force-length.[2] It is a set of two equal and opposite moments about the same axis separated by a distance (see Fig. 1) and can be an applied force or can arise from restraining warping at a point. A good description of the bimoment and its origins can be found in Ref. 24.

The governing differential equation [Eq. (2)] is third order and, hence, has geometric twist and twist rate boundary conditions. The possible boundary conditions are twist restrained $\phi_z = 0$ or twist free $T_s = 0$ and warping restrained $\phi_z' = 0$ or warping free $M_\omega = 0$.

Restraining the warping deformation causes the twist rate to be zero at the point of restraint. This causes a local effective torsional stiffening that affects the global torsional response of the beam, similar to boundary layers in fluid dynamics.

A Vlasov type cross section analysis was used in the current model. A thorough derivation of the equations and cross-sectional stiffnesses can be found in Ref. 1. A general Vlasov theory approach is presented to model a beam with extension, bending, torsion, warping, and transverse shear deformations. The result is a 9×9 stiffness matrix relating beam forces to beam displacements. By considering only symmetric beams with cross-ply webs subjected to bending and torsional loads, the 9×9 matrix is reduced to 5×5:

$$\begin{Bmatrix} N \\ M_x \\ -M_y \\ M_\omega \\ T_s \end{Bmatrix} = \begin{bmatrix} K_{11} & K_{12} & K_{13} & K_{14} & K_{15} \\ K_{21} & K_{22} & K_{23} & K_{24} & K_{25} \\ K_{31} & K_{32} & K_{33} & K_{34} & K_{35} \\ K_{41} & K_{42} & K_{43} & K_{44} & K_{45} \\ K_{51} & K_{52} & K_{53} & K_{54} & K_{55} \end{bmatrix} \begin{Bmatrix} W' \\ \phi_y' \\ \phi_x' \\ \phi_z'' \\ \phi_z' \end{Bmatrix} \tag{3}$$

Equation (3) is appropriate for bending and torsion of symmetric beams and extension and torsion of antisymmetric beams. For proper modeling of axial deformation in symmetric beams or bending in

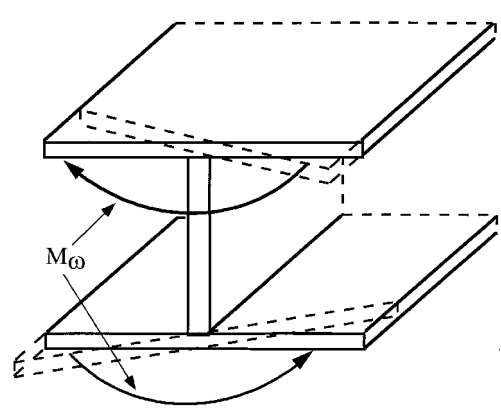

Fig. 1 Out-of plane warping and bimoment on I beam.

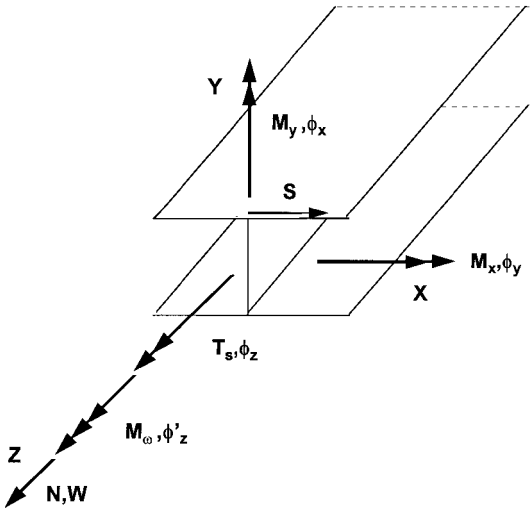

Fig. 2 Coordinate systems, forces, and displacements.

antisymmetric beams, the full 9×9 matrix would be necessary or a minimization process would be necessary to account for shear couplings. An example of this shear condensation is given in Ref. 22.

The beam coordinates, applied forces, and corresponding displacements are shown in Fig. 2. For general laminates and cross-sectional shapes, K is fully populated. In practical applications, many of the coefficients are zero. In an extreme case, an I beam with isotropic or cross-ply webs and flanges, the matrix is diagonal. The number of nonzero off-diagonal terms depends on the couplings present in the beam.

$$[K] = \begin{bmatrix} [K_{\text{Ext}}] & [K_{\text{Ext–Flap Bend}}] & [K_{\text{Ext–Chord Bend}}] & [K_{\text{Ext–Torsion}}] \\ [K_{\text{Ext–Flap Bend}}] & [K_{\text{Flap Bend}}] & [K_{\text{Flap Bend–Chord Bend}}] & [K_{\text{Flap Bend–Torsion}}] \\ [K_{\text{Ext–Chord Bend}}] & [K_{\text{Flap Bend–Chord Bend}}] & [K_{\text{Chord Bend}}] & [K_{\text{Chord Bend–Torsion}}] \\ [K_{\text{Ext–Torsion}}] & [K_{\text{Flap Bend–Torsion}}] & [K_{\text{Chord Bend–Torsion}}] & [K_{\text{Torsion}}] \end{bmatrix} \tag{11}$$

Finite Element Formulation

The specialized element is formulated through an energy method incorporating the principle of the stationary value of the total potential energy. First, the total potential energy is obtained from the strain energy and the potential of the external loads. The stationary condition is then applied to obtain the finite element equations. In the linear regime, the strain energy density expression for a beam undergoing extension, bending, torsion, and warping deformations is given by

$$\Pi_s^* = \tfrac{1}{2}[NW' + M_y\phi_x' + M_x\phi_y' + T_s\phi_z' + M_\omega\phi_z''] \tag{4}$$

If no shear is included, the bar displacements U' and V' can be substituted for ϕ_x and ϕ_y. This changes the strain energy expression to

$$\Pi_s^* = \tfrac{1}{2}[NW' + M_yU'' + M_xV'' + T_s\phi_z' + M_\omega\phi_z''] \tag{5}$$

Substituting the K matrix coefficients from Eq. (3), in terms of the bar forces and displacements, the strain energy becomes

$$\Pi_s^* = \frac{1}{2}\begin{pmatrix} K_{11}W'^2 + 2K_{12}V''W' + 2K_{13}U''W' + 2K_{14}\phi_z''W' \\ + 2K_{15}\phi_z'W' + K_{22}V''^2 + 2K_{23}U''V'' + 2K_{24}\phi_z''V'' \\ + 2K_{25}\phi_z'V'' + K_{33}U''^2 + 2K_{34}\phi_z''U'' + 2K_{35}\phi_z'U'' \\ + K_{44}\phi_z''^2 + 2K_{45}\phi_z'\phi_z'' + K_{55}\phi_z'^2 \end{pmatrix} \tag{6}$$

The potential of the external loads on the beam in terms of the same displacements is given by

$$\Omega = nW + v_xU + v_yV + t_s\phi_z + m_\omega\phi_z' \tag{7}$$

The lowercase letters are the applied (distributed) bar forces. To numerically discretize the equations, shape functions are then substituted for the bar displacements U, V, W, and ϕ_z. Two different types of shape functions were used. For the axial displacement, a three-node Lagrangian (C^0 continuous) representation was used. For bending and torsion, a two-node Hermitian (C^1 continuous) representation was used. The shape functions can be found in a finite element textbook, such as Cook.[25] By substituting for the bar displacements with the appropriate shape functions, the following expressions are obtained for the discretized displacements:

$$\{U\} = \{H\}^T \begin{Bmatrix} u_1 \\ u_1' \\ u_2 \\ u_2' \end{Bmatrix}, \qquad \{V\} = \{H\}^T \begin{Bmatrix} v_1 \\ v_1' \\ v_2 \\ v_2' \end{Bmatrix}$$
$$\{W\} = \{L\}^T \begin{Bmatrix} w_1 \\ w_2 \\ w_3 \end{Bmatrix}, \qquad \{\phi_z\} = \{H\}^T \begin{Bmatrix} \phi_{z1} \\ \phi_{z1}' \\ \phi_{z2} \\ \phi_{z2}' \end{Bmatrix} \tag{8}$$

The column vectors in Eq. (8) are the nodal displacements. These discretized displacements are substituted for the displacements in the strain energy density expression [Eq. (6)] and integrated over the beam length. A more compact matrix form results:

$$\Pi_s = \tfrac{1}{2}\{D\}^T[k]\{D\} \tag{9}$$

The potential of the external loads is placed in a similarly compact matrix form:

$$\Omega = -\{D\}^T\{R\} \tag{10}$$

The element stiffness matrix comprises 10 unique submatrices, one for each stiffness and coupling term. The element stiffness matrix, in terms of the 10 submatrices, is given by

There is a corresponding integral expression for each of the submatrices,

$$[K_{\text{Ext}}] = \int_0^L (\{L'\}[K_{11}]\{L'\}^T)\,dx \tag{12}$$

$$[K_{\text{Flap Bend}}] = \int_0^L (\{H''\}[K_{22}]\{H''\}^T)\,dx \tag{13}$$

$$[K_{\text{Chord Bend}}] = \int_0^L (\{H''\}[K_{33}]\{H''\}^T)\,dx \tag{14}$$

$$[K_{\text{Torsion}}] = \int_0^L (\{H'\}[K_{55}]\{H'\}^T + \{H''\}[K_{44}]\{H''\}^T + 2\{H'\}[K_{45}]\{H''\}^T)\,dx \tag{15}$$

$$[K_{\text{Ext–Torsion}}] = \int_0^L (\{L'\}[K_{15}]\{H'\}^T + \{L'\}[K_{14}]\{H''\}^T)\,dx \tag{16}$$

$$[K_{\text{Flap Bend–Torsion}}] = \int_0^L (\{H''\}[K_{25}]\{H'\}^T + \{H''\}[K_{24}]\{H''\}^T)\,dx \tag{17}$$

$$[K_{\text{Chord Bend–Torsion}}] = \int_0^L (\{H''\}[K_{35}]\{H'\}^T + \{H''\}[K_{34}]\{H''\}^T)\,dx \tag{18}$$

The stiffness coefficients in the remaining matrices are small or zero for the I-beam geometry and bending–torsion ply orientations considered. Expressions for these matrices are very similar to those in Eqs. (12–18). Likewise, had transverse shear been included, there would be additional submatrices for the shear degrees of freedom, each of similar form.

The potential of the external loads is given in terms of the load vector R. It is a stacked column vector of the nodal displacements,

$$\{R\} = \begin{Bmatrix} \{n_i\} \\ \{v_{yi}\} \\ \{v_{xi}\} \\ \{t_{si}\} \end{Bmatrix} \tag{19}$$

Similar to the element stiffness matrix k, there is also an integral expression for each of the terms in the vector of the external loads R:

$$\{n\} = \int_0^L \{L\}^T n(z)\,dz \tag{20}$$

$$\{v_y\} = \int_0^L \{H\}^T v_y(z)\,dz \tag{21}$$

$$\{v_x\} = \int_0^L \{H\}^T v_x(z)\,dz \tag{22}$$

$$\{t_s\} = \int_0^L (\{H\}^T t_s(z) + \{H'\}^T m_\omega(z))\,dz \tag{23}$$

The displacement vector $\{D\}$ in Eqs. (9) and (10) is a stacked column vector of the nodal displacements:

$$\{D\} = \begin{Bmatrix} \{w_i\} \\ \{v_i\} \\ \{u_i\} \\ \{\phi_{zi}\} \end{Bmatrix} \tag{24}$$

Summing the strain energy and the potential of the external loads yields the total potential energy

$$\Pi_p = \Pi_s + \Omega \tag{25}$$

Substituting the expressions for Π_s and Ω, a matrix equation for the element in terms of the element stiffness matrix, load vector, and displacement vector is obtained:

$$\Pi_p = \tfrac{1}{2}\{D\}^T[k]\{D\} - \{D\}^T\{R\} \tag{26}$$

Using the principle of the stationary value of the total potential energy, the following stationary condition is applied:

$$\frac{\partial \Pi_p}{\partial \{D\}} = \{0\} \tag{27}$$

This results in the standard discretized finite element equations,

$$[k]\{D\} = \{R\} \tag{28}$$

Having derived the finite element equations, some important observations can be made. This discretization includes the torsion stiffness, the warping stiffness due to Vlasov effects, and the warping–torsion coupling stiffness (often zero) in one submatrix, as shown in Eq. (15). Note that in a similar manner, the terms coupling torsion with other degrees of freedom must also be the sum of the warping coupling and the torsion coupling. This is a unique feature of the current research. Through the simple addition of the warping strain energy into the element strain energy, the Vlasov torsion is rigorously accounted for.

Comparison to Previous Method

From Eq. (3), the term that relates applied St. Venant torque and the twist deformation is K_{55}. Inclusion of warping effects was previously accomplished in Refs. 21–23 using a St. Venant torsion model by modifying this stiffness coefficient over part or all of the beam. One such approach, found in Ref. 23, was based on closed-form solutions to the governing differential equation for torsion. This approach was used in a previous rotor system aeroelastic analysis. Results for the current model will be compared to this approach. A brief overview of its formulation is presented here.

For a composite beam with a cross-ply web and identical flanges, subjected only to bending and torsional loads, the governing differential equation is found in Ref. 1 to be

$$K_{44}\phi_z''' - (K_{55})_r\phi_z' = -\bar{T} \tag{29}$$

where

$$(K_{55})_r = K_{55} - (K_{25}^2/K_{22}) \tag{30}$$

The reduced torsion stiffness reflects the increased compliance due to bending–torsion couplings. The general solution to Eq. (29) is

$$\phi_z = \left[\frac{\bar{T}}{(K_{55})_r}\right]z + A + B\sinh\lambda z + C\cosh\lambda z \tag{31}$$

where

$$\lambda = \sqrt{\frac{(K_{55})_r}{K_{44}}} \tag{32}$$

and where λ is a parameter that can be used to assess warping effects in a cross section. Accounting for beam length, the parameter λL is a good indicator of the importance of warping effects in a beam. Vlasov torsion effects diminish as λL grows large with respect to unity.

The arbitrary constants A, B, and C in Eq. (31) are found by substituting the boundary conditions into the general solution. The torsional response of the beam with a tip torque and warping restrained at the root and tip is given as

$$\phi_z = \frac{\bar{T}}{\lambda(K_{55})_r}\left[\lambda z - \sinh\lambda z + \frac{\cosh\lambda L - 1}{\sinh\lambda L}(\cosh\lambda z - 1)\right] \tag{33}$$

The stiffness modification in Ref. 23 is based on this equation and the classic St. Venant result for a beam with a tip torque, given by

$$\phi = Tz/GJ \tag{34}$$

To obtain the modified stiffness equation [Eq. (34)] is solved for GJ and ϕ is replaced with the expression in Eq. (33) to obtain

$$GJ(z) = z\lambda(K_{55})_r \Big/ \left[\lambda z - \sinh\lambda z + \frac{\cosh\lambda L - 1}{\sinh\lambda L}(\cosh\lambda z - 1)\right] \tag{35}$$

There are several conceptual and practical problems with this approach. First, the closed-form equation is for specific boundary conditions, in this case warping restrained at the root and tip. This is achieved by $GJ(z)$ becoming infinite near a restraint. In Eq. (35) the denominator contains an expression for $\phi(z)$, not $\phi'(z)$, and so the stiffness becomes infinite when the twist approaches zero, not when the twist rate approaches zero as the proper boundary conditions dictate. Also, the numerator is proportional to $(K_{55})_r$, rather than to K_{55}, to reflect the increase in compliance due to bending–torsion couplings. The result is used in a finite element stiffness matrix. Therefore, the compliance increase is accounted for twice, once analytically to obtain $GJ(z)$ and once numerically in the finite element analysis. There is no physical justification to support this.

In contrast, the current approach incorporates the warping effects directly into the element strain energy. In previous approaches, the torsion solution had to be known a priori, whereas in the current analysis, no prior knowledge is necessary. The restrictions on simple loadings, uniform geometries, and prespecified boundary conditions are thus removed. Instead of changing the torsion stiffness with an equation, the current model directly enforces the kinematic boundary conditions and uses the analytical stiffnesses in the finite element.

The Vlasov cross section model for torsion is often discretized with a three-node Lagrangian (C^0 continuity) polynomial representation. In this study, torsion is incorporated into the specialized beam finite element through Hermitian polynomials. Hermitian polynomials feature continuity of both twist and twist rate (C^1 continuity).

Table 1 Comparison of features of modified-*GJ* method and current formulation

Modified-*GJ* method	Current method
Numerical or analytical a priori solution necessary for analysis	No a priori solution needed
C^0 continuous shape functions	C^1 continuous shape functions allow warping moment to be carried from element to element
Warping boundary conditions approximated by equation	Geometric boundary conditions are directly enforced
Main diagonal stiffness terms altered by analysis	Calculated stiffnesses used
Analytical model changes with boundary condidions and loadings	Boundary conditions and loadings applied in solution

This allows the warping moment to vary across the finite element, similar to bending moments in a standard Hermitian bending representation. The warping is linked directly to the twist rate degree of freedom as in the governing differential equation and strain energy equation. Torsion is represented by two nodes and two degrees of freedom per node, ϕ and $\phi\prime$. For restrained warping, the $\phi\prime = 0$ boundary condition can be easily enforced. A comparison of features of the current model and the modified-*GJ* model is shown in Table 1.

Results

The new finite element was validated against closed-form solutions for I beams from Ref. 1 and detailed shell element solutions. The closed-form solutions were previously tested against experimental results, and good correlation was achieved. The I beams tested were graphite/epoxy; material properties are $E_L = 20.59 \times 10^6$ psi (Msi), $E_T = 1.42$ Msi, $G_{LT} = 0.89$ Msi, $\nu_{LT} = 0.42$, and ply thicknesses$= 0.005$ in.

A baseline uncoupled case was tested to check the accuracy of the new element. The results are plotted in Fig. 3. The beam has a 1×0.5 in. cross section, with $[0/90]_4$ layups in the flanges and the web. Note that the word symmetric in the layup description on each plot is with respect to the beam centerline. In other words, the first ply is on the inside of the flange for both the top and bottom. The beam is loaded with a unit tip torque and is clamped at the root with warping restrained at the root and tip. It can be seen that the new finite element can accurately predict this simple case, as the shell element solution, the closed-form solution, and the current model are nearly coincident. The shell element model contained 300 thin, shallow shell quadrilateral elements, with six degrees of freedom per element. The plot shown used eight beam elements for consistency with the other, more complex results presented. It should be noted that convergence is extremely rapid for the new element, and this baseline case was modeled to 98.4% accuracy with a single beam element compared to the closed-form solution.

Bending–torsion coupled cases were also tested to verify that the new element could not only model twist response but could also model both the bending due to torque loading and the twist due to bending loading. The beam considered had flange layups of $[0/90]_3[15]_2$ and a web layup of $[0/90]_4$. Results are shown for twist under a unit tip torque (in Fig. 4), for twist under a unit tip bending load (in Fig. 5), and for bending slope under a unit tip torque (in Fig. 6). In each plot, the current model coincides exactly with the closed-form solution. The modified-*GJ* solution is in error by a significant amount in each case. Note that the twist rate for the modified-*GJ* plots does not approach zero at the tip. The St. Venant character of the element is evident in the discontinuous twist rate between the first and second elements, at the 7.5-in. spanwise position. The current model is a smooth curve over the entire length of the beam due to the continuity of twist and twist rate. These figures show that the new model can accurately predict the torsion response and the coupled bending response as well.

To examine the versatility of the new element, the baseline cases were modified in beam geometry, boundary conditions, and loadings, to verify that it was capable of modeling these changes. The first test verifies the dependence of warping on aspect ratio, defined

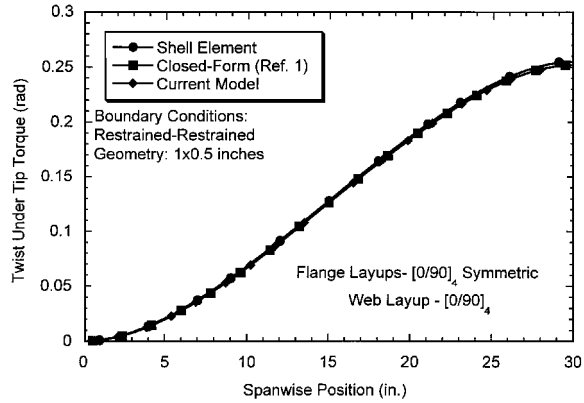

Fig. 3 Validation of twist distribution under tip torque for baseline uncoupled I beam.

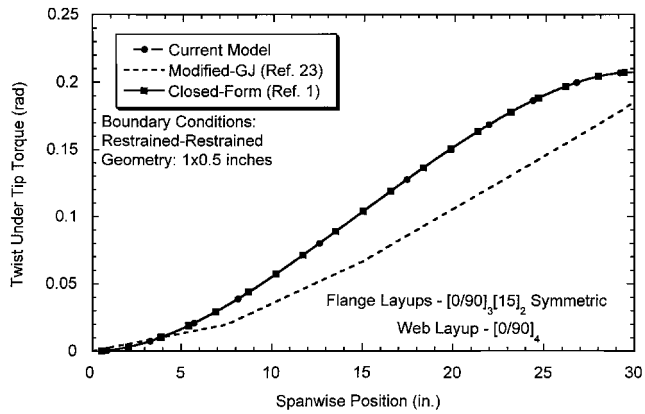

Fig. 4 Twist response of bending–torsion coupled beam under a tip torque.

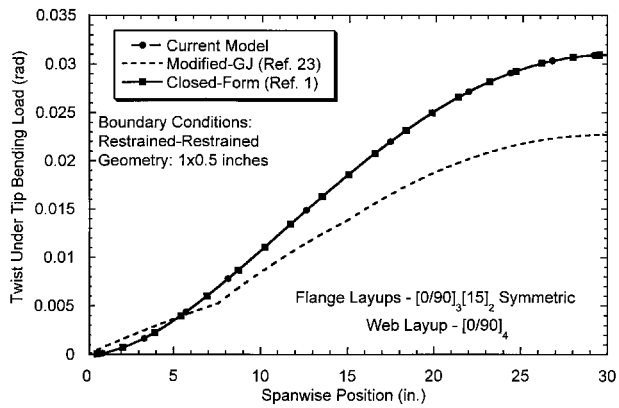

Fig. 5 Twist response of elastically coupled beam under tip bending load.

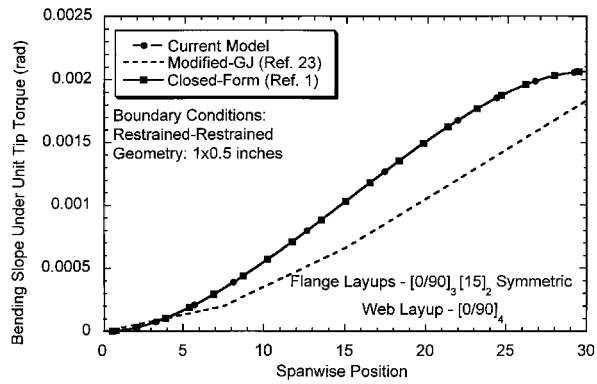

Fig. 6 Bending slope of elastically coupled beam under tip torque.

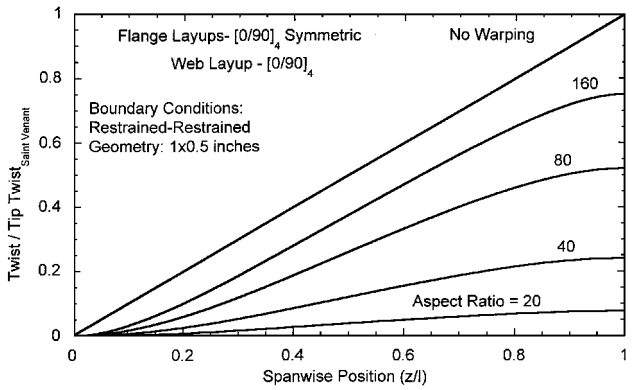

Fig. 7 Nondimensional effect of aspect ratio on torsional response with warping restrained at root and tip.

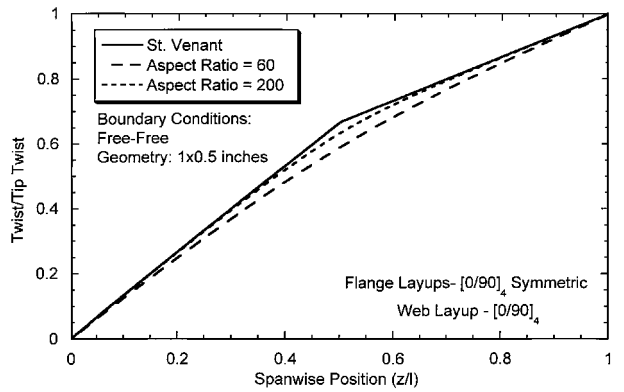

Fig. 8 Comparison of current model with St. Venant solution with midspan concentrated torque at different aspect ratios.

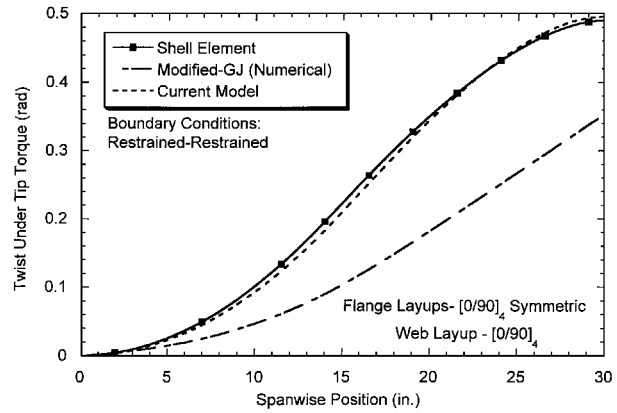

Fig. 9 Comparison of twist response of beam with tapered height and width under tip torque.

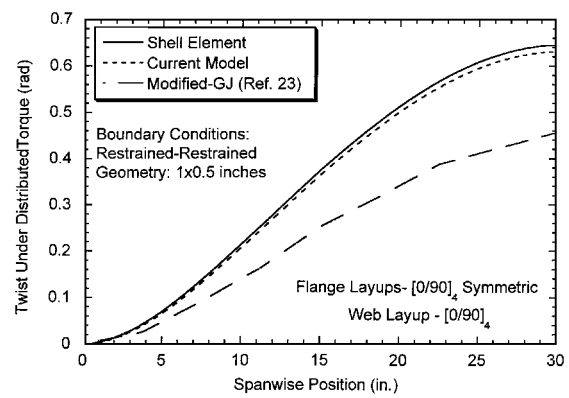

Fig. 10 Comparison of twist response of beam with distributed torsional loading.

as the length of the beam divided by its height. As aspect ratio increases, the effects of warping become smaller and the twist response approaches the St. Venant solution. Figure 7 shows the response of beams with different aspect ratios normalized to the tip twist response without warping restraint effects. When the aspect ratio is large (160), the slope of the twist curve is parallel in the middle to the St. Venant case. This shows the boundary-layer effect of the warping restraint, where only the first and last 20% are affected and about 60% in the midspan is not.

An interesting corollary to aspect ratio dependence is a comparison to St. Venant torsion for a midspan concentrated load. The St. Venant solution predicts a step change in twist rate at the point of load application. Element-to-element continuity of twist rate precludes step changes in the current model. A test case was examined to see if the new element would converge to the St. Venant solution if the warping was free at the root and tip. Note that with the current model changing the boundary condition to warping free requires only releasing the constraint on ϕ'. The result is shown in Fig. 8. At the smaller aspect ratio (long dashes), the tip twist deflection is identical, but the warping restraint effects prevent the step change in twist rate. The much higher aspect ratio (short dashes) is nearly coincident with the pure St. Venant result. From this it can be concluded that as the aspect ratio approaches infinity, the new element converges to the step change in twist rate predicted by St. Venant torsion theory.

One of the features of the new finite element is that it does not include any assumption about a uniform cross-sectional geometry over the span of the beam. To test the effectiveness of the current model on a nonuniform cross section, the model was used to analyze a beam with taper in both the spanwise and chordwise directions. The height was tapered linearly from 0.5 in. at the root to 0.25 in. at the tip. The width was 1.0 in. at the root, tapered linearly to 0.5 in. at 50% span, and widened linearly to 1.0 in. at the tip. This was considered to be a fairly arbitrary geometry that would test several different kinds of taper at once.

The beam was identical in loading, layup, and boundary conditions to the baseline case. Only the spanwise geometry was changed. Linearly tapered elements were obtained by integrating the element equations through fourth-order Gauss quadrature. Twist results under tip torques are shown in Fig. 9. The modified-*GJ* stiffnesses were obtained by curve fitting the shell element solution to a fifth-order polynomial and using the resulting $\phi(z)$ to obtain an equation similar to Eq. (35). The current approach models the twist response predicted by the shell element solution quite closely, where the modified-*GJ* method is in significant error. This indicates that the new element is capable of modeling changes in spanwise geometry and lends itself to methods such as Gauss quadrature. Developing a closed-form solution for a tapered case would be difficult. The shell element solution, though accurate, took about 90 s to run. Run times of less than 1 s were typical for the current model.

As a final validation test, spanwise load distributions were analyzed to show the improved versatility of the new finite element over the modified-*GJ* approaches. Figure 10 shows twist distribution with a distributed torsional load. Very close correlation is achieved between the new finite element and the shell element solutions. Therefore, it is also capable of modeling distributed loads.

Additional cases were tested to determine the effects of taper on warping restraint effects. The layups were cross ply as in the baseline case. Four taper cases were examined for each I beam: uniform, linearly decreasing taper, linearly increasing taper, and a neck taper where the geometry is tapered to a minimum in the center of the beam. The symbols at the bottom of Fig. 11 illustrate the taper geometries. For all tapered cases, the minimum dimension is one-half of the maximum dimension. For example, the first four bars show taper in the y direction (beam height). For the second bar (linearly decreasing taper), the height is 0.5 in. at the root and 0.25 in. at the tip (and a width of 1.0 in. throughout). The height of the bars in Fig. 11 is the percent tip deflection relative to the pure Saint Venant case. Taller bars indicate warping is less important; a height of 100% represents the St. Venant solution. When warping is restrained at the root and tip, the linearly increasing and linearly decreasing cases are identical. When warping is restrained at the

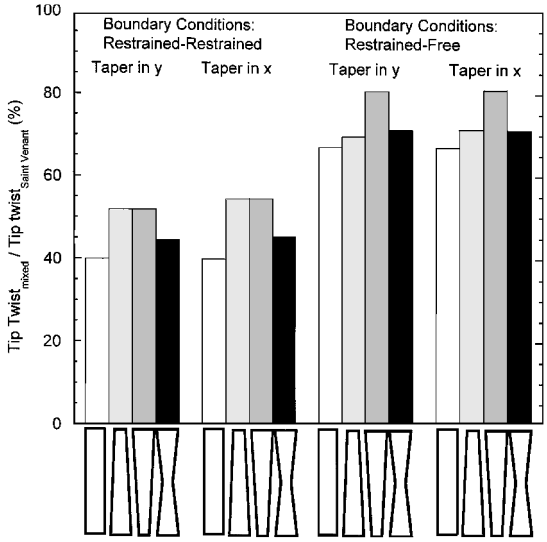

Fig. 11 Effects of width and height taper on warping restraint effects for different boundary conditions.

root only, the results are closer to St. Venant torsion for the linearly increasing case. This indicates that the cross-sectional geometry in the vicinity of the warping restraint determines the importance of warping restraint effects. More information is available on taper effects in Ref. 26.

Conclusions

1) A new finite element has been developed that is capable of modeling the kinematic boundary conditions associated with mixed torsion. It features C^1 continuity and only one additional degree of freedom per element over a three-node C^0 continuous model.

2) Validation with shell element models and closed-form solutions showed that results were indistinguishable from closed-form solutions with and without elastic couplings. Results for uniform and tapered cases showed excellent agreement with shell element results.

3) New model is an improvement in accuracy compared to current modified-GJ approach. For taper and nonuniform loads, the accuracy was improved by 25% with only one additional degree of freedom per element compared to a three-node Lagrange representation.

4) For computationally intensive analyses such as aeroelastic stability calculations, the current model provides a substantial improvement in accuracy and versatility over closed-form solutions at far less computational cost than a detailed shell element model.

5) Current model reduces to Saint Venant solution if warping parameter λL is sufficiently large.

Acknowledgments

The authors would like to thank the U.S. Army Research Office for supporting this project under Grant DAAH04-94-G-0206. The Technical Monitor is Gary Anderson.

References

[1]Chandra, R., and Chopra, I., "Experimental and Theoretical Analysis of Composite I-beams with Elastic Couplings," *Proceedings of the AIAA 32nd Structures, Structural Dynamics, and Materials Conference*, AIAA, Washington, DC, 1991.

[2]Harse, J. H., "The Four-Bladed Main Rotor System for the AH-1W Helicopter," *Proceedings of the 45th Annual Forum of the American Helicopter Society*, American Helicopter Society, Alexandria, VA, 1989, pp. 837–850.

[3]Bishop, H. E., and Dixon, P. G. C., "The Bearingless Main Rotor," *Journal of the American Helicopter Society*, Vol. 25, No. 3, 1980, pp. 15–21.

[4]McNulty, M., Jacklin, S., and Lau, B., "A Full-Scale Test of the McDonnell Douglas Advanced Bearingless Rotor in the NASA Ames 40- by 80-Ft Wind Tunnel," *Proceedings of the 49th Annual American Helicopter Society Forum*, American Helicopter Society, Alexandria, VA, 1993, pp. 1535–1544.

[5]Norman, T. R., Cooper, C. R., Fredrickson, C. A., and Herter, J. R., "Full-Scale Wind Tunnel Evaluation of the Sikorsky Five-Bladed Bearingless Main Rotor," *Proceedings of the 49th Annual American Helicopter Society Forum*, American Helicopter Society, Alexandria, VA, 1993, pp. 1507–1523.

[6]Enenkl, B., and Klöppel, V., "Design Verification and Flight Testing of a Bearingless Soft Inplane Tail Rotor," *Proceedings of the 42nd Annual Forum of the American Helicopter Society*, American Helicopter Society, Alexandria, VA, 1986, pp. 1113–1126.

[7]Vlasov, V. Z., *Thin-Walled Elastic Beams*, National Science Foundation and U.S. Dept. of Commerce, Washington, DC, 1961, Chaps. 1, 2 (translated from Russian).

[8]Gjelsvik, A., *The Theory of ThinWalled Bars*, Wiley, New York, 1981, Chaps. 1–4.

[9]Bauld, N. R., and Tzeng, L. S., "A Vlasov Theory for Fiber-Reinforced Beams with Thin-Walled Open Cross-Sections," *International Journal of Solids and Structures*, Vol. 20, No. 3, 1984, pp. 277–297.

[10]Chandra, R., and Chopra, I., "Structural Response of Composite Beams and Blades with Elastic Couplings," *Composites Engineering*, Vol. 2, Nos. 5–7, 1992, pp. 347–374.

[11]Chandra, R., and Chopra, I., "Structural Behavior of Two-Cell Composite Rotor Blades with Elastic Couplings," *AIAA Journal*, Vol. 30, No. 12, 1992, pp. 2914–2921.

[12]Bauchau, O. A., and Chiang, W., "Dynamic Analysis of Bearingless Tail Rotor Blades Based on Nonlinear Shell Models," *Journal of Aircraft*, Vol. 31, No. 6, 1994, pp. 1402–1410.

[13]Bauchau, O. A., "A Beam Theory for Anisotropic Materials," *Journal of Applied Mechanics*, Vol. 52, June 1985, pp. 416–422.

[14]Kosmatka, J. B., "A Nonlinear Theory for Spinning Anisotropic Beams Using Restrained Warping Functions," AIAA Paper 93-1303, April 1993.

[15]Kosmatka, J. B., "Extension, Bending, and Torsion of Anisotropic Beams with Initial Twist," *Proceedings of the AIAA/ASME/ASCE/AHS 30th Structures, Structural Dynamics, and Materials Conference*, AIAA, Washington, DC, 1989, pp. 1799–1806 (AIAA Paper 89-1364).

[16]Crawley, E. F., and Dugundji, J., "Frequency Determination and Non-Dimensionalization for Composite Cantilever Plates," *Journal of Sound and Vibration*, Vol. 72, No. 1, 1980, pp. 1–10.

[17]Jensen, D. W., Crawley, E. F., and Dugundji, J., "Vibration of Cantilivered Graphite/Epoxy Plates with Bending-Torsion Coupling," *Journal of Reinforced Plastics and Composites*, Vol. 1, July 1982, pp. 254–269.

[18]Lee, S. W., and Kim, Y. H., "A New Approach to the Finite Element Modelling of Beams with Warping Effect," *International Journal for Numerical Methods in Engineering*, Vol. 24, March 1987, pp. 2327–2341.

[19]Stemple, A. D., and Lee, S. W., "Finite-Element Model for Composite Beams with Arbitrary Cross-Sectional Warping," *AIAA Journal*, Vol. 26, No. 12, 1988, pp. 1512–1520.

[20]Yuan K., Friedmann, P., and Venkatesan, C., "A New Aeroelastic Model for Composite Rotor Blades with Straight and Swept Tips," *Proceedings of the AIAA 33rd Structures, Structural Dynamics, and Materials Conference*, AIAA, Washington, DC, 1992, pp. 1371–1390 (AIAA Paper 92-2259).

[21]Nixon, M. W., "Analytical and Experimental Investigations of Extension-Twist-Coupled Structures," M.S. Thesis, School of Engineering and Applied Science, George Washington Univ., Washington, DC, May 1989.

[22]Tracy, A. L., and Chopra, I., "Aeromechanical Stability of a Bearingless Composite Rotor in Forward Flight," *Proceedings of the AIAA 34th Structures, Structural Dynamics, and Materials Conference*, AIAA, Washington, DC, 1993, pp. 63–79.

[23]Tracy, A. L., and Chopra, I., "Aeroelastic Analysis of a Composite Bearing less Rotor in Forward Flight with Improved Warping Modeling," *Proceedings of American Helicopter Society Aeromechanics Specialists Conference*, American Helicoptor Society, Alexandria, VA, 1994, pp. 7.4-1–7.4-17.

[24]Murray, N. W., *Introduction to the Theory of Thin-Walled Structures*, Oxford Univ. Press, Oxford, England, UK, 1984, pp. 1–11.

[25]Cook, R. D., Malkus, D. S., and Plesha, M. E., *Concepts and Applications of Finite Element Analysis*, Wiley, New York, 1989, pp. 96–101.

[26]Floros, M. W., "Finite Element Modeling of Open-Section Composite Beams with Warping Restraint Effects," M.S. Thesis, Dept. of Aerospace Engineering, Pennsylvania State Univ., University Park, PA, Aug. 1996.

R. K. Kapania
Associate Editor